C228

JPL PUBLICATION 82-61

End-to-End Imaging Information Rate Advantages of Various Alternative Communication Systems

Robert F. Rice

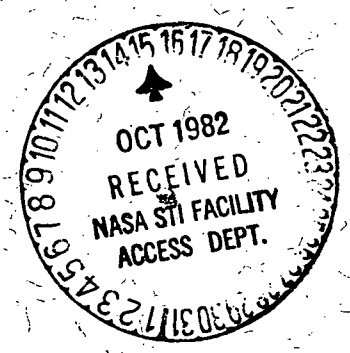

September 1, 1982

National Aeronautics and
Space Administration

Jet Propulsion Laboratory
California Institute of Technology
Pasadena, California

JPL PUBLICATION 82-61

End-to-End Imaging Information Rate Advantages of Various Alternative Communication Systems

Robert F. Rice

September 1, 1982

National Aeronautics and
Space Administration

Jet Propulsion Laboratory
California Institute of Technology
Pasadena, California

The research described in this publication was carried out by the Jet Propulsion Laboratory, California Institute of Technology, under contract with the National Aeronautics and Space Administration.

ACKNOWLEDGMENT

The author wishes to offer particular thanks to Edward Hilbert of Goodyear and to Jun-Ji Lee and Alan Schlutsmeyer of the JPL Information Processing Research Group for their numerous technical contributions to this work. He also wishes to express his gratitude to the many colleagues whose related technical work or programmatic support over the past decade has particularly influenced the general acceptance of these concepts within the space program. These include Bob Breshears, Ed Greenberg, Adrian Hooke, Don Johnson, Kuang Liu, Marv Perlman, and Don Rea.

The research described in this paper was carried out by the Information Processing Research Group of the Jet Propulsion Laboratory, California Institute of Technology.

ABSTRACT

This paper provides an end-to-end analysis comparing the efficiency of various deep space communication systems which are required to transmit both imaging and a typically error sensitive class of data called general science and engineering (gse) over the classic Gaussian channel. The approach jointly treats the imaging and gse transmission problems, allowing comparisons of systems which include various channel coding and data compression alternatives. Actual system comparisons include an "Advanced Imaging Communication System" (AICS) which exhibits the rather significant advantages of sophisticated data compression coupled with powerful yet practical channel coding. For example, under certain conditions the improved AICS efficiency could provide as much as two orders of magnitude increase in imaging information rate compared to a single channel uncoded, uncompressed system while maintaining the same gse data rate in both systems. Additional details describing AICS compression and coding concepts as well as current efforts to apply them are provided in support of the system analysis.

TABLE OF CONTENTS

Figures

Tables

END-TO-END IMAGING INFORMATION RATE ADVANTAGES OF VARIOUS ALTERNATIVE COMMUNICATION SYSTEMS

I. INTRODUCTION

There have been substantial advances in the communication capability of deep space missions since Mariner IV first sent data back from Mars at 8 1/3 bits/sec in 1964. For example, the recent Voyager spacecraft were able to communicate from Jupiter at 115 Kbits/sec, an improvement of over four orders-of-magnitude. Most of this monumental gain was accomplished by improvements in the basic components and parameters of the telecommunication system which improved the received signal-to-noise ratio (e.g., increased antenna diameters, better pointing accuracy, higher transmitter frequencies, etc.). Processing and coding have, until quite recently, played a relatively minor role. However, while these early improvements in signal-to-noise ratio were clearly cost-effective, further increments have become progressively more difficult and costly. Thus with the dramatic advances in solid state technology, the joint advantages of information processing (e.g., data compression) and channel coding entered an era of practical consequence.

This paper traces this evolution by providing an end-to-end analysis which illustrates the sometimes huge performance difference that can exist between deep space communication systems. As such the results have been a strong advocate for both data compression and other processing as well as a specific channel coding configuration now nearing NASA standardization. Specifically we provide a means of comparing the efficiency of various communication systems which are required to transmit both imaging and a typically error sensitive class of data called here general science/engineering (gse) over a Gaussian channel (the usual space channel, no bandwidth limitations). This approach jointly treats the imaging and gse transmission problems and allows practical comparisons of systems which include various channel coding and data compression alternatives. Utilizing this technique, comparisons of five alternative communication systems are provided. These comparisons illustrate that the capability to communicate imaging information of the most sophisticated system is from 20 to 100 times that of the most basic system. Exhibiting such distinct performance differences, these systems probably span the full range of potential performance available today for communicating imaging and gse data over

the classic space channel. The relative performance of other systems not treated here would fit within this range and can be obtained by simple derivations using the same techniques or in many cases by parameter substitution.

The system comparisons and principal results of this paper are presented in Section II. Additional background supporting the data compression and channel coding assumptions are provided in Sections III and IV respectively. The remainder of this section is primarily devoted to introducing the method and philosophy of system comparison.

Error Rate Disparity

Clearly, a communication system which must transmit more than one form of data must satisfy the minimum transmission error rate requirements of all the data. Performance comparisons of various systems to accomplish this task must account for these constraints. This is precisely the situation considered here. Generally speaking, gse data can be classified as strictly error sensitive data although there may be slight differences in the error vulnerability of various types. Imaging data on the other hand may or may not be error sensitive depending on the method of image representation. The effect of transmission errors on uncompressed grey scale images tends to be significantly less than the effect of errors on compressed images (or gse data) for many techniques, and almost universally for algorithms employing adaptive processing and control. We will assume this "classic" error vulnerability since we are interested in identifying the maximum gains possible from processing and compression. The direct consequence of this assumption is that both gse and compressed imaging data require a much lower transmission error rate (to avoid unacceptable damage) than does uncompressed imaging.

Systems Considered, Method of Comparison

The systems considered here represent an evolution of communication systems developed for planetary missions. The first four systems represent steps in that evolution (not chronological) based on the assumption that imaging data would be uncompressed and that gse data would be either nonexistent or at least always a small percentage of the total information rate. In that sense a comparison of systems 1-4 demonstrates distinct step-by-step improvements in efficiency. As noted

above part of the motivation of this paper is to display the relative efficiencies of these systems to transmit both uncompressed imaging and gse data.†

Certainly there are variations to systems 1-4 and modifications which might include various compression algorithms. It is a straightforward matter to present comparisons of such systems by the approaches developed here. However, we elect to demonstrate the potential advantages of data compression by providing comparisons with system 5. System 5, called an "Advanced Imaging Communication System" (AICS) in Refs. 1 and 2, is the result of an end-to-end design aimed at transmitting all forms of data efficiently. It includes both adaptive data compression and channel coding which eliminates the data rate penalty associated with a requirement for low transmission error rates. Comparisons with system 5 should indicate roughly the maximum gains that are presently available from the use of data compression.

Method of comparison. Each of the first four systems will be separately viewed as "baseline systems." It is assumed in all cases that the parameters of each system are selected so that the minimum error rate requirements for all data are simultaneously satisfied. The gse data rate, r, will be fixed in all systems as a fraction of the total data rate in the baseline so that with R_B denoting the image data rate in the baseline

$$f = \frac{r}{r + R_B} = \begin{array}{l}\text{gse fraction of total} \\ \text{data rate in baseline}\end{array} \qquad (1)$$

Then, the imaging data rate of each alternative system, R_n, will be compared with that available in the baseline so that

$$\frac{R_n}{R_B} = \begin{array}{l}\text{Imaging rate advantage of} \\ \text{system n: a function of f}\end{array} \qquad (2)$$

†For many potential missions the performance of accurate navigation may require "information" from specific star field images to be transmitted in addition to the imaging and non-imaging science (gse). At low overall data rates the communication of full uncompressed images for this purpose could make a noticeable impact on the effective data rate available for science. However, it will be shown in a later paper that it is reasonable to assume compression factors of 100:1 or more for such "optical navigation" images, thus making their impact negligible and an unnecessary concern in this paper.

This is summarized in Fig. 1. Note that an improvement in imaging data rate by β in any system means roughly the ability to transmit β times as many images with equivalent information content as those transmitted in the baseline.

Section II will introduce the five candidate system configurations and present the comparative analysis described by (1) and (2) in graphical form. Supportive information and background for image compression are provided in Section III and for the channel coding options in Section IV.

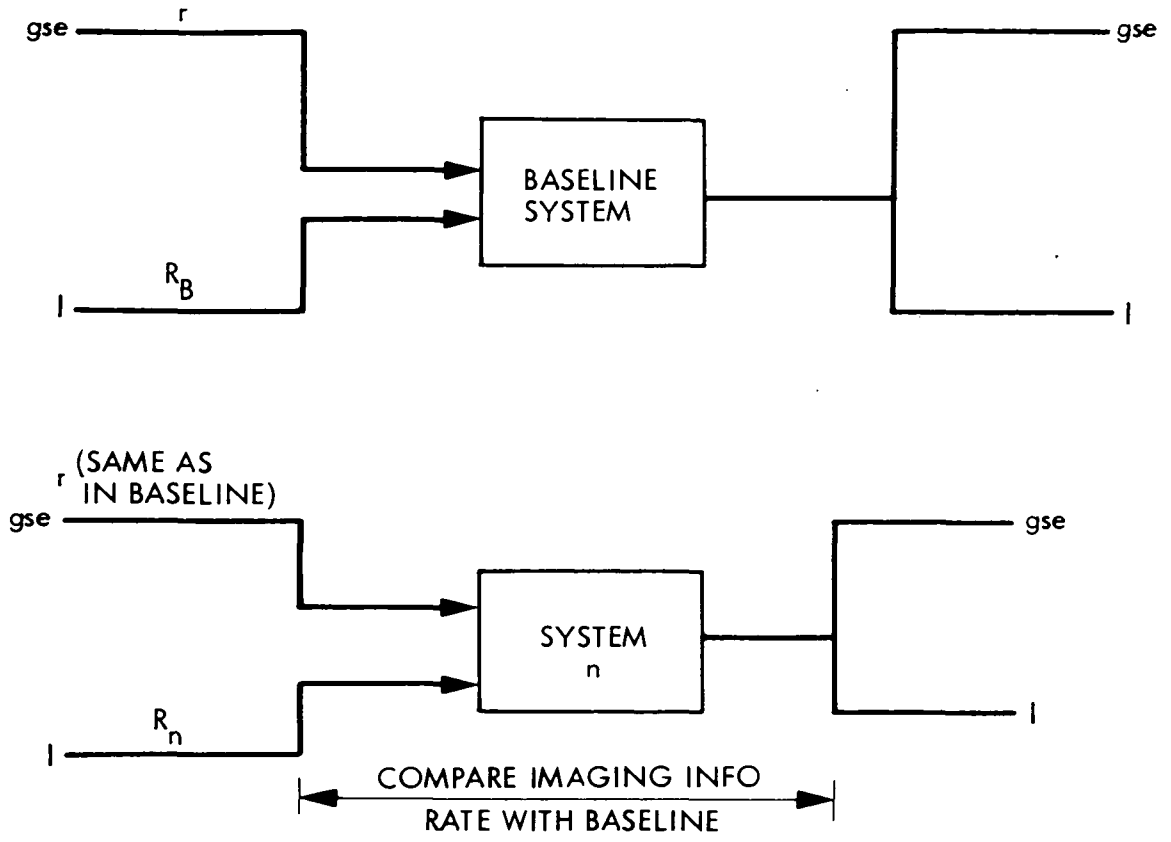

$\frac{r}{r + R_B}$ = f = GSE FRACTION OF TOTAL INFORMATION RATE IN BASELINE

$\frac{R_n}{R_B}$ = IMAGING RATE ADVANTAGE OF SYSTEM n: A FUNCTION OF f

Fig. 1. Method of System Comparisons.

II. SYSTEM COMPARISONS

Each of the systems considered will be introduced while treating system 1 as a baseline system (that is, the system to compare others to). In all cases presented here we will assume PSK modulation and ideal coherent receiver operation. The necessary performance curves for the various channel options can be found for convenience in Section IV where further information concerning non-ideal receiver conditions is noted.

System Descriptions: System 1 as Baseline

System 1 is simply the familiar "uncoded channel" as diagrammed in Fig. 2.

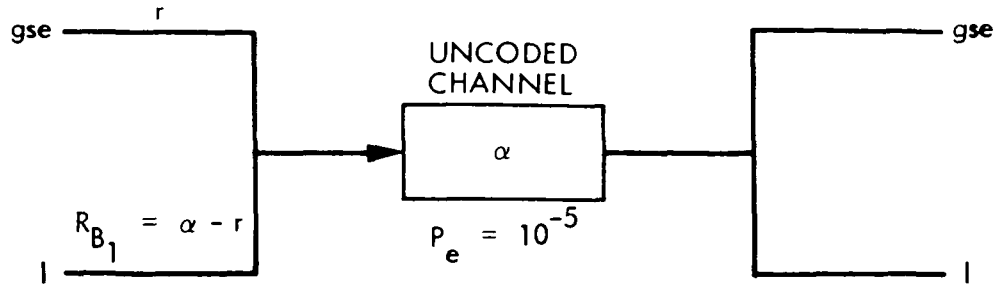

Fig. 2. System 1, Uncoded Channel.

Assuming this is the baseline system, gse data rate is fixed at an average rate of r bits/sec where $r/\alpha = f$ and α is the total available bit rate for the channel. Then $R_{B_1} = \alpha - r$ is the imaging information rate available in the baseline system 1.

Assuming we fix antenna size, transmitter power, etc., α is determined solely by the allowed bit error probability, $\overline{P}_b$. The error sensitive gse data confines this choice to be low. For comparison purposes we will use $\overline{P}_b = 10^{-5}$. The exact choice will have little impact on the end results and 10^{-5} has in practice been an acceptable value. This operating point is obtained at a signal-to-noise ratio of roughly 9.7 dB.

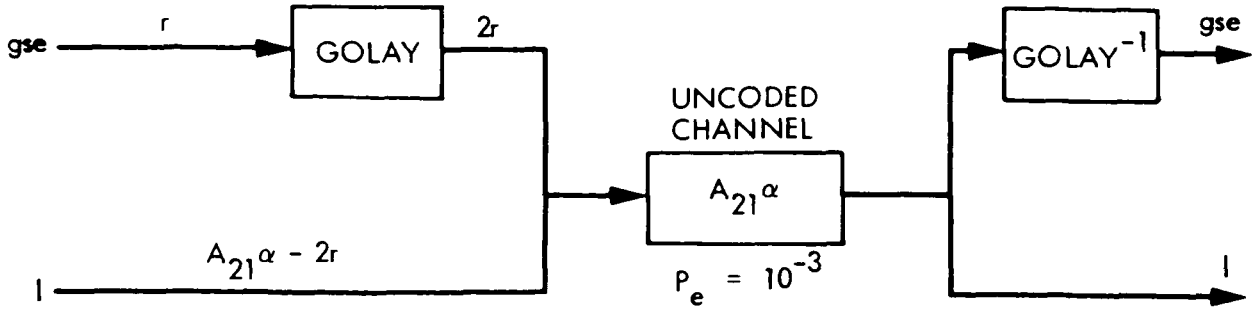

Fig. 3. System 2 (Uncoded/Golay) vs. Uncoded Baseline.

As shown in Fig. 3, Golay block coding is applied to gse data before transmission over the "inner" uncoded channel. The (24,12) Golay code assumed is a slightly modified form of the familiar (23,12) code.[3] Thus r parity bits are required for each r information bits.

Because of the additional protection of gse data, the uncoded channel in this system may be operated at higher error rates and hence higher transmission rates. Specifically, transmission rate on the uncoded channel portion may be increased provided that the net gse error rate is around 10^{-5} or less and uncompressed or subsampled imaging is not substantially degraded. To meet this objective, bit error rate requirements of imaging have historically been $\overline{P}_b \leq 5 \times 10^{-3}$.

This gse-constrained operating point for the inner uncoded channel occurs in the range of 5×10^{-3}. We will assume a $\overline{P}_b = 10^{-3}$ in the graphical examples. From uncoded channel performance curves the $\overline{P}_b = 10^{-3}$ operating point occurs at roughly 6.8 dB. This satisfies the requirements for imaging noted above. Thus the uncoded channel in system 2 may be operated at 2.9 dB above that in system 1 or at a rate which is $A_{21} \approx 1.95$ times that in system 1. Operating points substantially above this point would rapidly damage gse data. This leaves an imaging rate of $R_{B_2} = A_{21}\alpha - 2r$ in system 2.

Note that for the channels over which imaging data passes $A_{ij} = 1/A_{ji}$ will henceforth denote the rate improvement factor of system i over system j.

System 3, Convolutional/Viterbi. A block diagram of system 3 is shown in Fig. 4. System 3 looks much like the baseline system except that all data is first coded by a convolutional coder, and then decoded using Viterbi decoders. There are many variations that may fit different mission situations.[4] For the purpose of presenting graphical results here, we will assume the same principal code used on

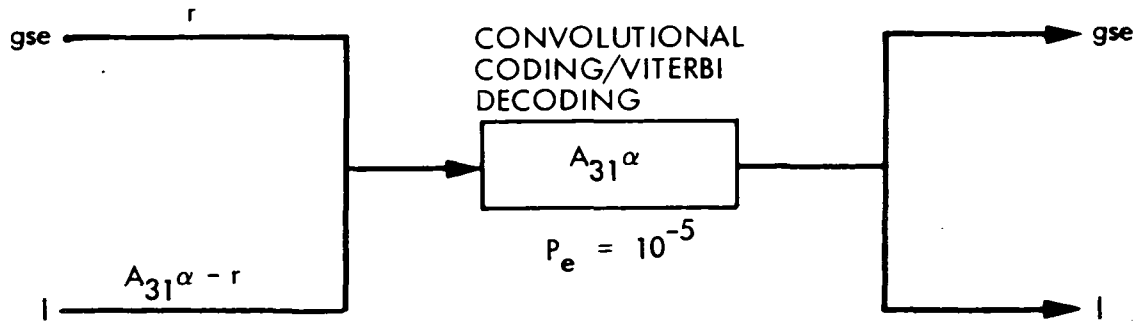

Fig. 4. System 3 (Conv/Viterbi) vs. Uncoded Baseline.

the Voyager missions to Jupiter and Saturn, a constraint K = 7, ν = 2 code with 3 bits of receiver quantization. Graphs for other options can easily be obtained by modifying input parameters. The various performance options for convolutional codes were first elaborated on in Ref. 5 and should still serve as a valuable guide.

From the K = 7, ν = 2 performance curves under ideal receiver operating conditions (Section III) we see that a $\overline{P}_b \leq 10^{-5}$ can be achieved with a signal-to-noise ratio which is 4.9 dB lower than an uncoded link. Thus data can be communicated at $A_{31} \approx 3.09\,\alpha$ bits/sec in system 3 while meeting the error rate requirements of both imaging and gse data.

System 4, Voyager. A block diagram of system 4 appears in Fig. 5.

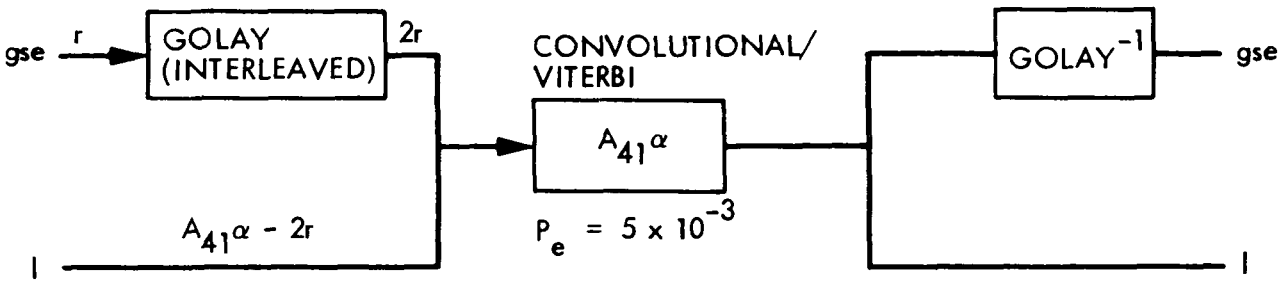

Fig. 5. System 4 (Conv/Viterbi-Golay) vs. Uncoded Baseline.

This system configuration is basically the Voyager communication system (also called the Jupiter/Saturn communication system in Refs. 1 and 2). It looks much like system 2, Uncoded/Golay, except that the inner channel is the more powerful convolutional/Viterbi and the Golay must be interleaved to be effective.[3]

We will assume that the inner channel can be operated at up to a $\overline{P}_b = 5 \times 10^{-3}$ while maintaining an adequately low $\overline{P}_b$ on gse data. Again it is unimportant to worry about precise operating points. The main differences between systems are much more significant. Using the K = 7, ν = 2 performance curves we have $A_{41}\alpha \approx 5.5\alpha$ bits/sec as the maximum transmission rate of the convolutional channel. This leaves $A_{41}\alpha - 2r$ bits/sec for imaging.

System 5, AICS. The last system considered here has been called the "Advanced Imaging Communication System" (AICS) for which a full description as originally conceived can be found in Ref. 2. Further background on the elements

of AICS and for the assumptions used in the system comparisons of this section is provided in Sections III and IV. A block diagram is shown in Fig. 6.

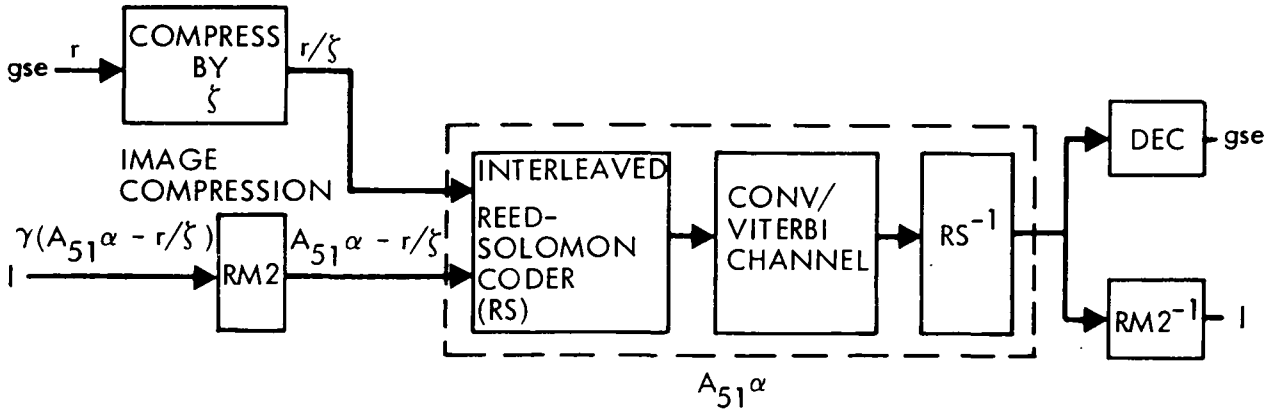

Fig. 6. System 5 (AICS) vs. Uncoded Baseline.

In this system all data pass through an interleaved Reed-Solomon coder before entering the same convolutional/Viterbi channel just discussed. The net result is that virtually error-free data can be communicated at rates up to very nearly that at which the convolutional/Viterbi channel alone obtains a 5×10^{-3} error rate. That is, $A_{51} \approx A_{41}$.

With this kind of channel, there is no problem with communicating error sensitive data. In Fig. 6, we have assumed that gse data is compressed by some factor ζ without any loss in true information. This appears quite feasible and in any event ζ should be a system parameter even if we set it equal to 1. In the graphic results the case of $\zeta = 1$ or $\zeta = 2$ will be included. Observe in Fig. 6 that with the actual gse data rate again fixed at r bits/sec there now remain $A_{51}\alpha - r/\zeta$ bits/sec in system 5 to be applied to imaging.

Although any image compression algorithm can fit within the structure of Fig. 6 we will principally assume the capability of RM2[2] which was developed specifically to provide the scientific user and mission designer with extensive flexibility to maximize information return. These characteristics are more fully treated in Section III. For the moment we require only the net gain which can be associated with representing images by data compression.

RM2 was evaluated for planetary flyby missions by imaging scientists[6] who concluded that it offered an information rate advantage of 4-to-6 times compared to alternatives of no compression or subsample algorithms. These conclusions were substantiated in a similar more recent study for the NASA End-to-End Data System (NEEDS).[7],[8] A more sophisticated use of RM2 flexibility and/or a sensor with registered multispectral bands might realistically raise the maximum advantage to 10:1 for some mission situations. To account for these possibilities we will assume a range of RM2 or other image data compression information rate advantages, denoted by γ, of 4:1 to 10:1.

In addition to the above numbered assumed range we will also include two special cases now in the process of implementation. The first is a planned reprogramming of the current Voyager II spacecraft flight data system to incorporate a near noiseless coding of image data for a January 1986 encounter of Uranus. Based on current expectations, a gain of $\gamma = 3$ will be assumed for the Voyager image compression.[9]-[13] The full structure of Fig. 6 will be made possible in this application by the existence of an as yet unused hardware Reed-Solomon encoder. The latter was incorporated just prior to launch as a backup for a potential X-band failure mode.

A second similar application of near noiseless coding has been incorporated into the Galileo (1985 launch) imaging system for which γ has been fixed at 2.5.[14] We will assume the full structure of Fig. 6 although actually the Reed-Solomon coding will, at this time, be applied only to imaging due to its late consideration in mission planning. Observe that the Galileo compressor, the Voyager compressor and RM2 are related by the use of Universal Noiseless Coding techniques described in Refs. 9 - 13.

Referring back to the diagram in Fig. 6 we see that

$$\gamma(A_{51}\alpha - r/\zeta) \tag{3}$$

is the effective imaging data rate for AICS, system 5.

Derivation of Imaging Rate Advantages

For each system just described we wish to obtain a more useful form of the ratio R_n/R_B given in (2). This requires no more than basic algebra. We will

illustrate the procedure here for AICS only. Equations for all systems, including different baseline choices, are given in Table 1.

From Figs. 1 and 2 we have

$$f = r/\alpha \tag{4}$$

$$R_B = \alpha - r + r(1 - f)/f \tag{5}$$

then from Fig. 6 and (3)

$$R_5 = \gamma(A_{51}\alpha - r/\zeta)$$

$$= \gamma(A_{51}\alpha\frac{r}{f} - r/\zeta)$$

$$= \frac{\gamma(A_{51} - f/\zeta)}{1 - f} R_B \tag{6}$$

The same approach can be followed for other systems. Similarly, picking a new baseline is no more complicated. The only difference is to now let α be the "imaging channel" rate for the selected baseline. Imaging channel refers to those channel elements over which imaging data passes. It does not exclude gse data.

Equations for Computing Imaging Rate Advantages

The necessary equations are shown in Table 1. Note that the rate factor $A_{ij} = 1/A_{ji}$ now more generally refers to the increase in transmission rate of the imaging channel of system i over that of system j. Observe that the f = 0 condition is really a discontinuity point for some of the systems because gse requirements would not constrain channel operating points. This fact is not noted in Table 1 or subsequent graphs but will be treated later.

A complete listing of the A_{ij} used here is given in Table 2. These may be derived from the channel performance curves given in Section IV.

Table 1. Equations for Computing Imaging Rate Advantages.

Assumed Baseline System	Imaging Rate Advantage Factor Above Baseline				
	System 1 Uncoded	System 2 Uncoded Golay	System 3 Conv/ Viterbi	System 4 Conv/Viterbi-Golay	System 5 AICS
System 1 Uncoded	1	$\frac{A_{21}-2f}{1-f}$	$\frac{A_{31}-f}{1-f}$	$\frac{A_{41}-2f}{1-f}$	$\frac{\gamma(A_{51}-f/\zeta)}{1-f}$
System 2 Uncoded/ Golay	$\frac{A_{12}-f(1-A_{12})}{1-f}$	1	$\frac{A_{32}-f(1-A_{32})}{1-f}$	$\frac{A_{42}-f(2-A_{42})}{1-f}$	$\frac{\gamma[A_{52}-f(1/\zeta-A_{52})]}{1-f}$
System 3 Conv/ Viterbi	$\frac{A_{13}-f}{1-f}$	$\frac{A_{23}-2f}{1-f}$	1	$\frac{A_{43}-2f}{1-f}$	$\frac{\gamma(A_{53}-f/\zeta)}{1-f}$
System 4 Conv/ Viterbi-Golay	$\frac{A_{14}-f(1-A_{14})}{1-f}$	$\frac{A_{24}-f(2-A_{24})}{1-f}$	$\frac{A_{34}-f(1-A_{34})}{1-f}$	1	$\frac{\gamma[A_{54}-f(1/\zeta-A_{54})]}{1-f}$

- gse data rate held fixed in all systems as fraction f of total information rate in Baseline System.
- $A_{ij} = 1/A_{ji}$ = Rate Advantage in operating imaging channel of system i over imaging channel of system j (see Figs. 2-6).

Table 2. Tabulation of the A_{ij}.

System Number		Imaging Channel Rate Improvement Factor A_{ij}				
		j →				
		1	2	3	4	5
i ↓	1	1.0	0.51	0.32	0.18	0.19
	2	1.95	1.0	0.63	0.35	0.38
	3	3.09	1.58	1.0	0.56	0.60
	4	5.50	2.82	1.78	1.0	1.07
	5	4.90	2.50	1.59	0.88	1.0

Graphical Results

Plots of equations in Table 1 are shown in Figs. 7 - 10 using f as a parameter.[15],[16] Included are AICS graphs assuming the Voyager compressor ($\gamma = 3$, $\zeta = 1$), the Galileo compressor ($\gamma = 2.5$, $\zeta = 1$) and RS/Viterbi alone ($\gamma = 1$), ($\zeta = 1$).

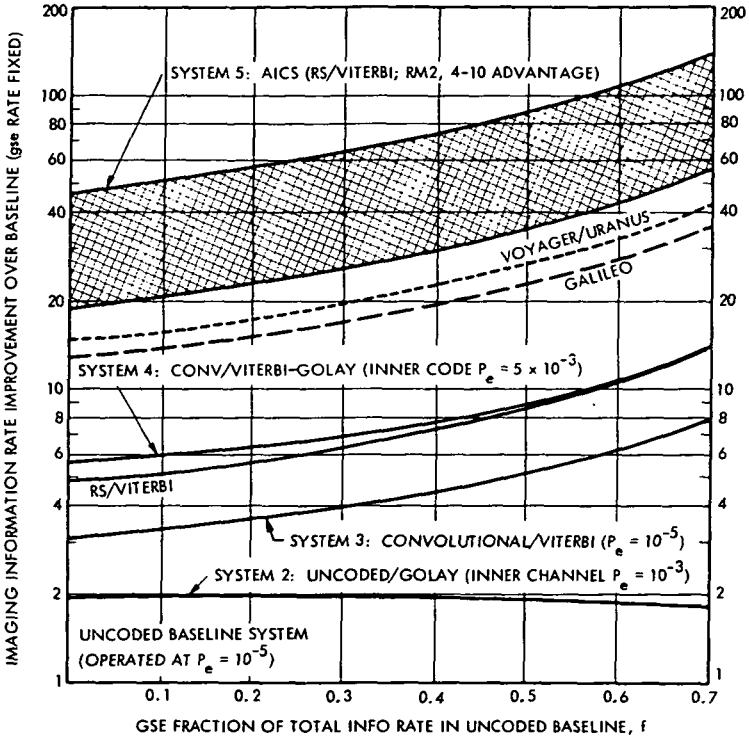

Fig. 7. System 1 Baseline: Uncoded.

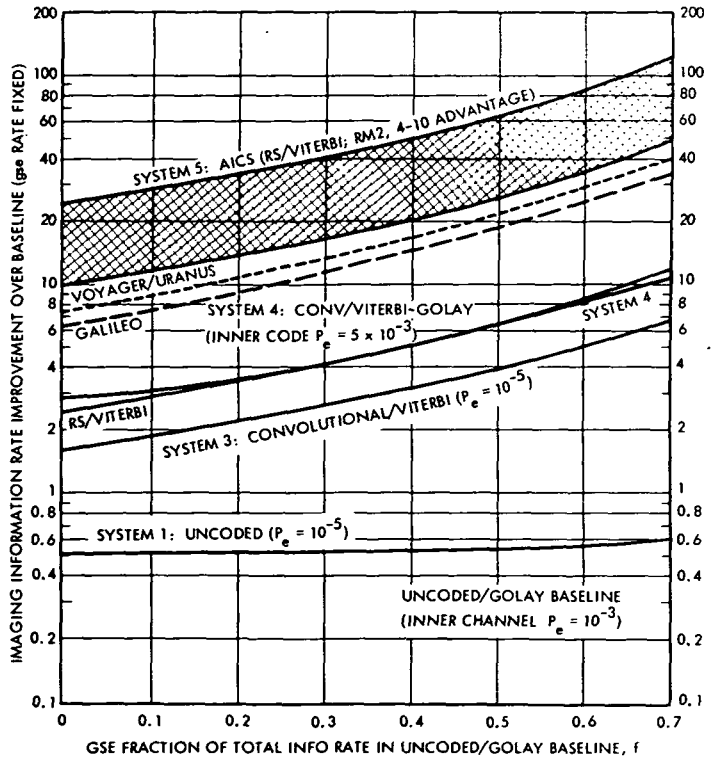

Fig. 8. System 2 Baseline: Uncoded/Golay.

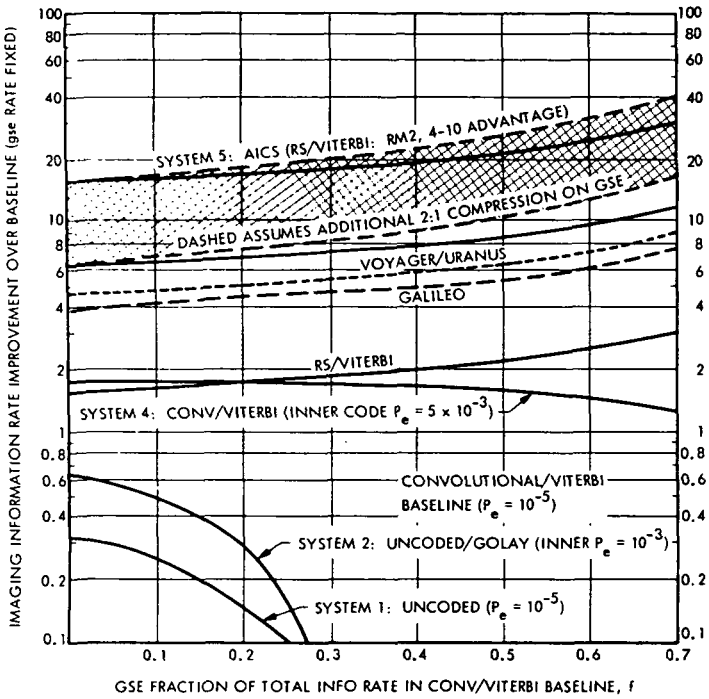

Fig. 9. System 3 Baseline: Conv/Viterbi.

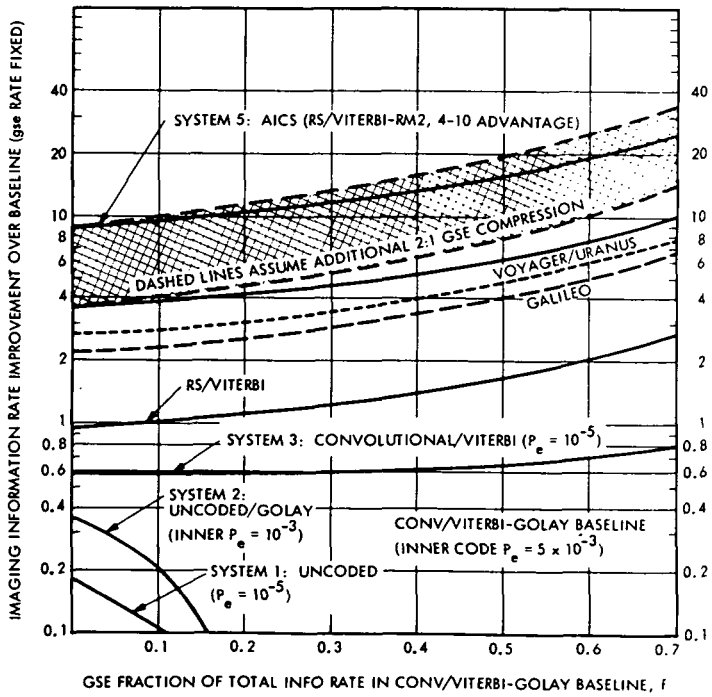

Fig. 10. System 4 Baseline: Conv/Viterbi-Golay.

Example 1. Suppose that the uncoded channel (system 1) was considered the baseline communication system. Upon sizing up the power, antenna, etc., it was concluded that 1 Kbit/sec was available at the required $\bar{P}_b = 10^{-5}$. Science instruments required at least r = 500 bits/sec to be reasonable, leaving 500 bits/sec for imaging. Then

$$f = \frac{500}{1000} = 0.5, \; R_B = 500 \text{ bits/sec} \tag{7}$$

The graphs in Fig. 7 compare the relative amount of imaging information rate with the R_B = 500 bits/sec in the baseline under the constraint that the gse data rate is the same (500 here) in all systems. From Fig. 7 with f = 0.5 we see the following imaging information rate advantages in Table 3. Given AICS and 18500 bits/sec or more of imaging instead of 500 it is likely that the allocation to gse data would increase since it would constitute now less than 3 percent of the total.

Table 3. Imaging Rate Advantages, Example 1

System	Approximate Factor, R_n/R_B	Imaging Information Rate (bits/sec)
Uncoded/Golay	1.9	950
Convolutional/Viterbi	4.5	2250
Conv/Viterbi-Golay	8.6	4300
RS/Viterbi	9.0	4500
AICS	37 to 90	18500 to 45000

Example 2. Now start with a more powerful baseline system, the Voyager communication system. Assume that the available data rate for imaging and gse (at acceptable error rates) is 5 Kbits/sec. This is similar to the situation which would have been faced if X-band failed near Saturn during the actual Voyager mission. Let f = 0.5 again so that the gse data rate is r = 2500 bits/sec. Using Fig. 10 we see that if we assume no gse data compression, AICS offers an imaging rate advantage of between 6.5 and 16 (16250 and 40000 bits/sec respectively). If in addition we assume a not unreasonable 2:1 gse compression, the rate advantage factors increase to between 8 and 20 (20000 and 50000 bits/sec respectively).

Special Case, No gse

A gse fraction of the total data rate, f, equal to zero results in a special case for uncoded system 1 and the convolutional/Viterbi system 3 since gse error rate requirements no longer constrain the channel. Assuming that uncompressed imaging requirements for channel fidelity remain unchanged, it is easy to see that system 1 becomes equivalent to system 2 and system 3 becomes equivalent to system 4.

One could also consider removing the uncompressed imaging constraint on channel fidelity for systems 1-4, trading off increasing degradation from bit errors for an increased transmission rate. This is, of course, a familiar trade-off which has received considerable attention in the literature over the years, with and without data compression. Some of these efforts were worthwhile investigations reflecting real trade-offs within a limited set of system options. However, it does little to alter the relative position of AICS in the graphs of Figs. 7-10.

Inspection of the ideal performance curves for the Viterbi-decoded convolutional link in Section IV shows that to achieve a data rate improvement factor of only 1.25 would require accepting images degraded by a 1/20 bit error rate, certainly not a paying proposition. In fact, the current Deep Space Network Viterbi decoders have shown some difficulty with node synchronization at low signal-to-noise ratios corresponding to error rates exceeding 5×10^{-3}.[17] Thus in reality the questionable 25 percent gain in rate may not even be achievable.

Turning to the uncoded channel we see from Section IV that at a signal-to-noise ratio of roughly 2.8 dB the concatenated channel provides "virtually error-free" communication, whereas a user of the uncoded link must contend with a bit error rate exceeding 1/50. But AICS data compression can provide almost perfect images at factors of 3 to 4:1 and images of roughly equivalent quality at factors of 6 to 8:1.

Now take the error rate-versus-data rate trade-off on the uncoded link to an extreme. By accepting the consequences of a 1/10 bit error rate on uncompressed images means that data rate can be improved by a not insignificant factor of 2.75. AICS could, however, provide compressed images of equivalent highly degraded quality with factors in the vicinity of 40 to 50:1. It is hardly fruitful to debate the precision of this statement or all the in-between cases. The rather significant advantage of the completely user-controllable (see Section III) AICS rate/quality trade-off via data compression and the concatenated channel should be self-evident.

III. IMAGE COMPRESSION FOR DEEP SPACE EXPLORATION

The system analysis leading to the graphical results in Section II required only simple algebra but relied on the assumption of performance parameters based on experimental results, analysis, and common sense. This section lends further support to these assumptions by providing additional detail and historical perspective to the image data compression developments of AICS, system 5. Discussions will seek to remain at a tutorial level with emphasis on providing information useful in a system context.

These discussions will realistically presume negligible channel interaction since "virtually error-free" communication is a practical consequence of the AICS concatenated Reed-Solomon/convolutional-Viterbi channel. This is treated further in Section IV where the various channel performance curves are presented.

Performance Characteristics

The usual source coding problem of finding the best way to code an image with a prescribed number of bits is only a subset of the source coding problem considered in the AICS development. The buffer problem, loosely stated, involved seeking a means of providing a user the capability to distribute a fixed number of bits over a sequence of many images in a way which maximizes his scientific information return (imaging and non-imaging). Although such a problem will hardly yield to rigorous theoretical analysis, simply considering the obvious role of the scientific user in planning imaging sequences leads to a powerful and practical source coding structure.

The basic philosophy behind the AICS source coding is to provide an extensive range of adaptivity at all levels of coding. At the level of user intervention, this means giving the user extensive capability to trade off rate and fidelity within an imaging sequence or from sequence-to-sequence. On a first order basis this capability is provided by the performance characteristics illustrated in the non-rigorous diagram of Fig. 11. Shown is a plot of image quality-versus-the bits/image reduction factor (compression) compared to an initial standard digital representation. Image quality is a difficult if not impossible term to quantify and we provide no magic formula to explicitly define it here. The quality measure shown in Fig. 11 is simply a composite of characteristics derived from many comparative

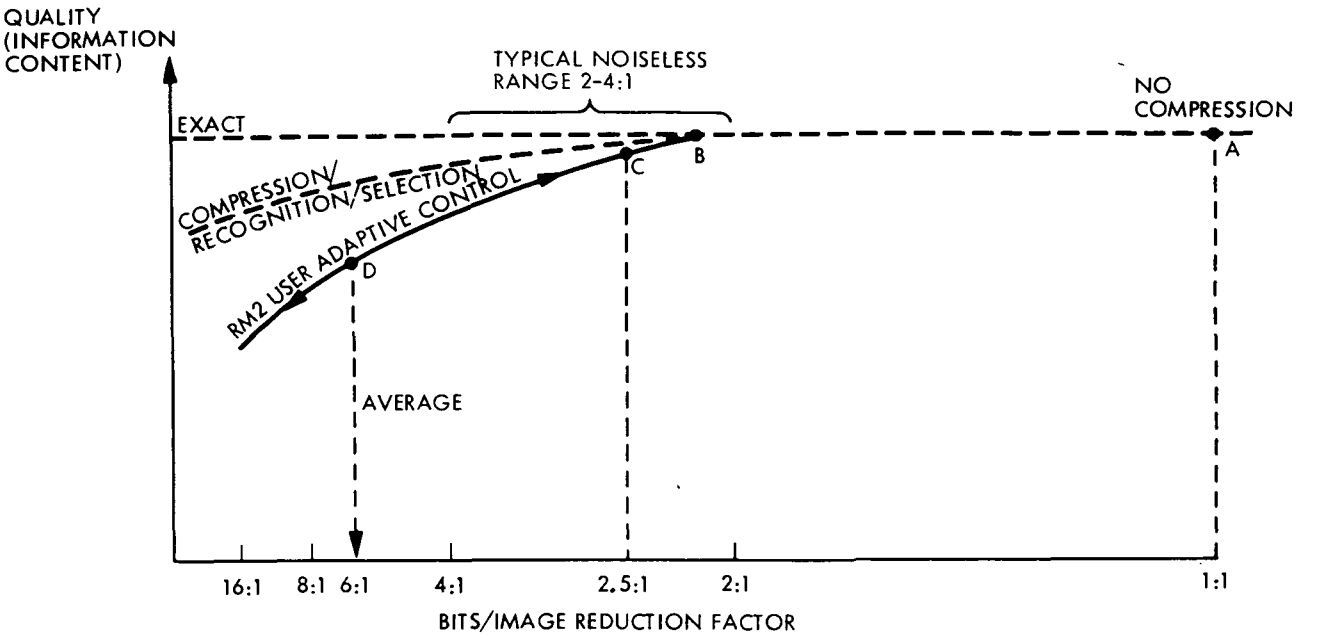

Fig. 11. Image Rate/Quality Trade-Off.

studies involving both subjective and quantitative measures of interest to the scientific investigator. Although we will later provide specific examples the general characteristics will suffice for our system arguments.

Noiseless Coding. First consider several well defined operating points on the graphs of Fig. 11. Point A represents the operating point for a system which uses no data compression. The corresponding quality of an image represents the best that a "given" digital camera system can provide. Point B corresponds to the application of "noiseless coding"[9]-[13] to image data, resulting in exact reconstruction, thus yielding precisely the same quality as for the original uncompressed data. Such noiseless coding results in data-dependent compression ratios of from 4:1 for low detail images to 2:1 or less for detailed images. Point B is an example for a fairly detailed image. The uncertainty in the achievable compression factor poses an operational problem since the timing of images cannot be arbitrarily changed. This can be partly or wholly offset when large buffers are available but the best approach is to recognize that, except for exceptional cases, a constraint of completely noiseless image coding for all images is an unnecessary burden as we will discuss below. The major observation at this point is that a rate advantage of at least 2 to 4:1 should be obtainable from data compression.

Rate/Quality trade-off. The performance graph starting at B in Fig. 11 and running through C and D represents the rate/quality trade-off available to a user of the RM2 algorithm first described as an element of AICS.[2] RM2 allows any compression factor to be selected for each image with the not surprising general characteristic that more bits applied to an image (lower compression factor) mean better quality up to the point where noiseless reconstruction occurs (near the image differential entropy). This continuous trade-off is provided by a globally adaptive rate allocation and control procedure.[2],[18] The latter allows a limited number of bits to be focused on image features having special fidelity requirements as discussed later.

Consider a basic application of the rate quality trade-off in Fig. 11. If only a single compression rate were allowed because of built-in operational constraints then that rate (or compression factor) would need to satisfy the most demanding mission requirements. This is much the same argument as the gse channel fidelity requirements directing the operation of communication systems 1-4 in Section II. This is precisely the situation for the Galileo mission to Jupiter. Image quality must, for at least some of the data, fully live up to the capability of the camera system. Thus, a compression factor of 2.5:1 (i.e., 3.24 bits/picture element) was chosen to ensure near-perfect images. Such an operating point corresponds to point C in Fig. 11. But at such low compression factors RM2 can be simplified to a one-dimensional form called BARC.[14] The latter has been implemented as part of the Galileo imaging system.

Two separate studies by imaging scientists[6]-[8] generally concluded that almost all per image scientific objectives could be derived from RM2 images coded at compression factors of 4:1 (i.e., 2 bits/picture element) although, as noted above, the near-perfect fidelity of a lower compression factor would be desirable under some conditions.

On the other hand there were some forms of data identified for which per image objectives could be met with considerably higher compression factors of 6 to 10:1. Using fewer bits-per-image for less demanding tasks should leave more bits to apply to tasks having more stringent fidelity requirements. Then, on a first order basis the broad performance curve provides the scientific user with a potential for fine tuning imaging sequences to either reduce the number of bits actually needed

or to more effectively utilize a fixed number. For example, an imaging sequence for which all images were coded at 3.0 bits/picture element (b/p) might be well approximated in science value by one in which only 20 percent were coded at 3.0 b/p, 30 percent at 2.0 b/p, 30 percent at 1.0 b/p and 20 percent at 0.5 b/p. This is an average of 1.6 b/p, providing an additional gain of nearly 2:1 (or 5:1 overall). Assuming a fixed number of bits-per-image sequence this improved efficiency could be used to roughly double the number or type of images (e.g., more planetary coverage, more spectral bands, more frequent images) thus increasing the science return. The availability of a continuous performance curve means that such trade-offs could be based on the most recent a priori knowledge of expected data characteristics, the user's current understanding of the fidelity he can expect at a given rate, and perhaps an updated list of scientific objectives (flight time for a deep space mission typically takes several years).

These arguments have implicitly sought to achieve maximum utilization of a given camera system. In so doing, the quality of any particular image is always presumed less than or equal to that resulting without compression. However, full utilization of these rate quality trade-offs should really begin with camera design before launch. The higher efficiency should allow greater capability to be incorporated in the basic design (e.g., higher resolution, more spectral bands). From this system point of view, data compression can yield better quality – not less.

Further pursuit of this line of thought is shown in the comparative photos of the same scene in Fig. 12. The image labeled "compressed" is clearly better than the one labeled "uncompressed." This unexpected result is because both images have been coded to the same number of bits. Whereas the uncompressed image simply indicates the basic capability of a low-resolution camera, the compressed image is an imperfect but good approximation to the output of a higher-resolution camera. The efficiency of data compression in this case materializes as better quality within a given image.

Global rate allocation. The basic RM2 control structure treats an image as an array of subimages (e.g., 32 x 32 picture elements) and first surveys these subimages to determine their "data activity" A_1, A_2, ..., A_N as illustrated in Fig. 13.

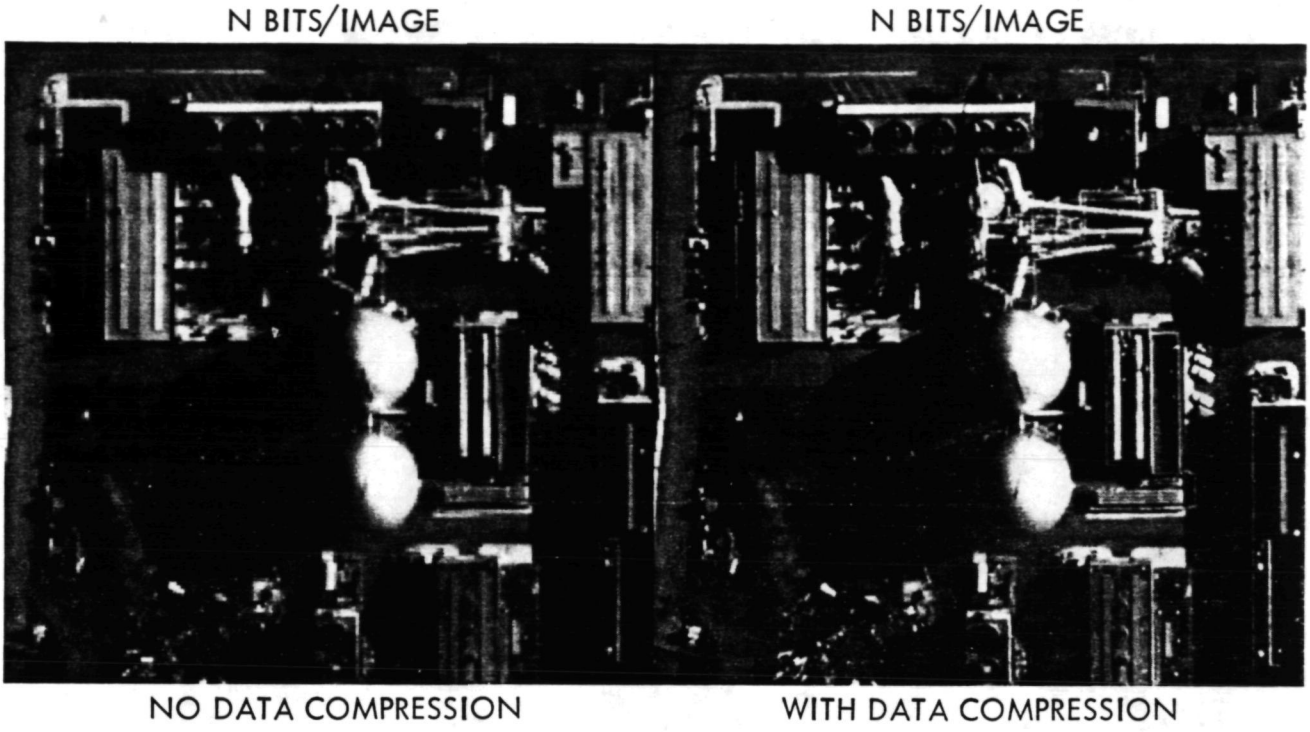

Fig. 12. Better Quality with Data Compression.

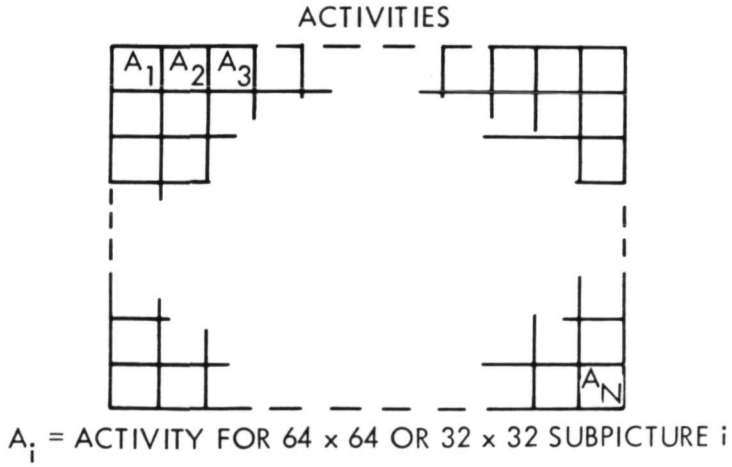

Fig. 13. Array of Data Activities.

The A_i may be computed "on the fly" as data is loaded into memory. These measures of activity directly relate to the relative need of each subimage for the limited number of bits available for the complete image. An internal algorithm[2] will allocate the total number of bits available for an image frame to the subimages in a way that reflects this need. More active subimages generally receive more bits than the less active subimages. Just as indicated for complete images in Fig. 11, more bits applied to a given subimage i mean better quality up to the point at which noiseless coding occurs (equal to A_i). This natural emphasis can be quite effective on large images with distinct variations in data activity throughout. The global rate allocation need not be restricted to individual images but can be applied to any sequence of images for which buffering is available.

Now extend this concept by assuming that pattern recognition is used to classify the same subimages (in one image or an image sequence) into data classes C_0, C_1, and C_2 as illustrated in Fig. 14. C_1 and C_2 might be classes of particular scientific interest whereas C_0 denotes all other data. The image quality in the C_1 and C_2 areas may be emphasized while maintaining the prescribed bits/image or bits/sequence simply by artificially boosting the natural activity measures for those regions. The rate allocation algorithm will, unknowingly, cause more bits (and hence quality) to flow to those subimages at the expense of subimages that did not get an artificial increase in their activity. Going in the other direction, if the information from a particular data class can be communicated with very few bits by

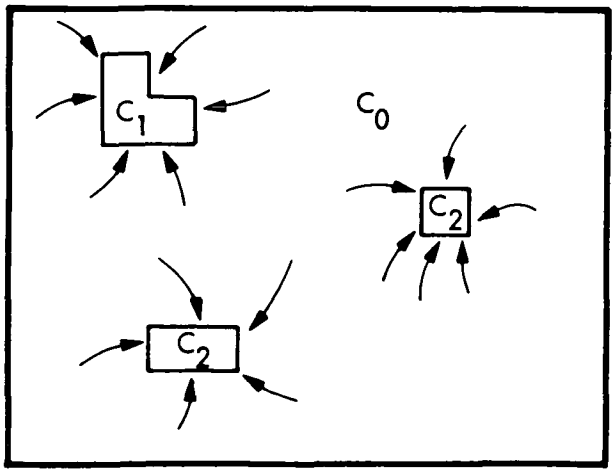

Fig. 14. Classification-Directed Rate Control.

extracting and communicating parameters only, then the unused bits can be simply reallocated to all other regions requiring image representation. A simple example of this occurs when an image consists of 50 percent planetary satellite and 50 percent black space. By simply identifying where black space is, the effective rate for image representation of the satellite itself can be doubled. Additional applications to reconnaissance from a military remotely-piloted vehicle are given in Ref. 18.

This classification-directed image compression clearly offers a potential for further improvements in the rate advantages of on-board information processing. As an aid to intuition, its effect may be viewed as moving the rate control performance upward to the dashed curve in Fig. 11. The overall net advantage is, at this time, speculative and is highly dependent on how broadly classification and parameter extraction can be applied. The global rate control structure of RM2 provides a practical mechanism for bridging the gap between pure information extraction and pure image representation.

Certainly, the Section II assumption that compression/processing can reduce data rate requirements for the representation of image information by 4:1 to 10:1 is a fair, and perhaps, conservative one.

The global rate allocation structure provides an additional subtle advantage when we again recall that a deep space mission does not consist of imaging alone. As noted in Section II a deep space investigation will consist of both imaging data and equally important general science and engineering data (gse). The information content of this class of data can vary considerably (many instrument outputs are bursty in nature). Efficient coding of gse data can thus produce a corresponding, and sometimes significant, variability in the overall gse output data rate. This can easily be accommodated by the image rate control structure when the average gse data rate is a small fraction of the total available data rate. Image or image sequence rate allocations are merely shifted up or down to absorb the changing gse requirements. An example is given in Ref. 2.

Classic quality comparisons. The preceding discussions should make clear that the overall source coding problem for this application is much more than simply coding individual images at some fixed rate. Total performance must be evaluated from a mission point of view. However, the performance of RM2 has been evaluated by more familiar approaches on several occasions. Figure 15 compares the rate in

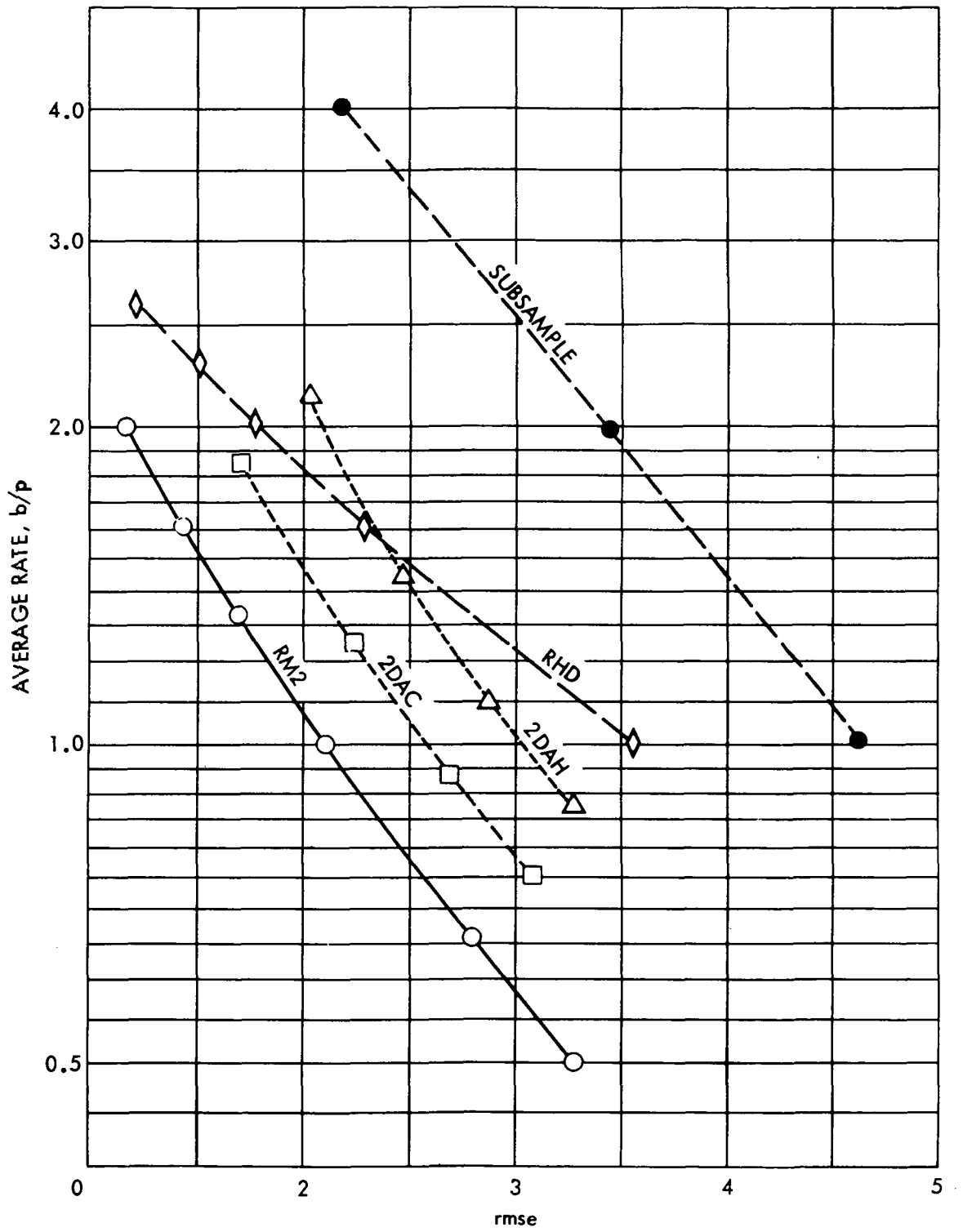

Fig. 15. Rate Versus Rmse.

bits/picture element (b/p) versus root-mean-square-error (rmse) performance of RM2 against several more familiar approaches to image coding.[19] Comparisons were made with both two-dimensional Hadamard (2DAH) and cosine (2DAC) adaptive algorithms (floating rate), a fixed-rate hybrid algorithm called randomized-Hadamard-dpcm (RHD)[20] and simple subsampling routines. The results shown are for one heavily cratered landscape selected by imaging scientists from the 1971 Mariner Mercury flyby.[2],[6] The 2DAH, 2DAC and RHD algorithms were fine tuned for the image and the selected rate. RM2 shows a decided advantage over all algorithms while providing the additional features noted earlier.

More recently RM2 was compared against a fixed-rate hybrid cosine/dpcm algorithm being implemented for an army remotely-piloted vehicle program.[21] RM2 was applied to the same sequence of six representative reconnaissance images selected by the military and shown in Fig. 16. Averaged over all the images the optimized cosine/dpcm algorithm required an average of 1.7 times as many bits to represent the images with the same rmse as RM2. This factor varied from roughly 1.2 on very noisy images to 2.5 on a detailed but highly correlated "crossroads" image. A graph of rmse comparisons for the latter image is shown in Fig. 17.

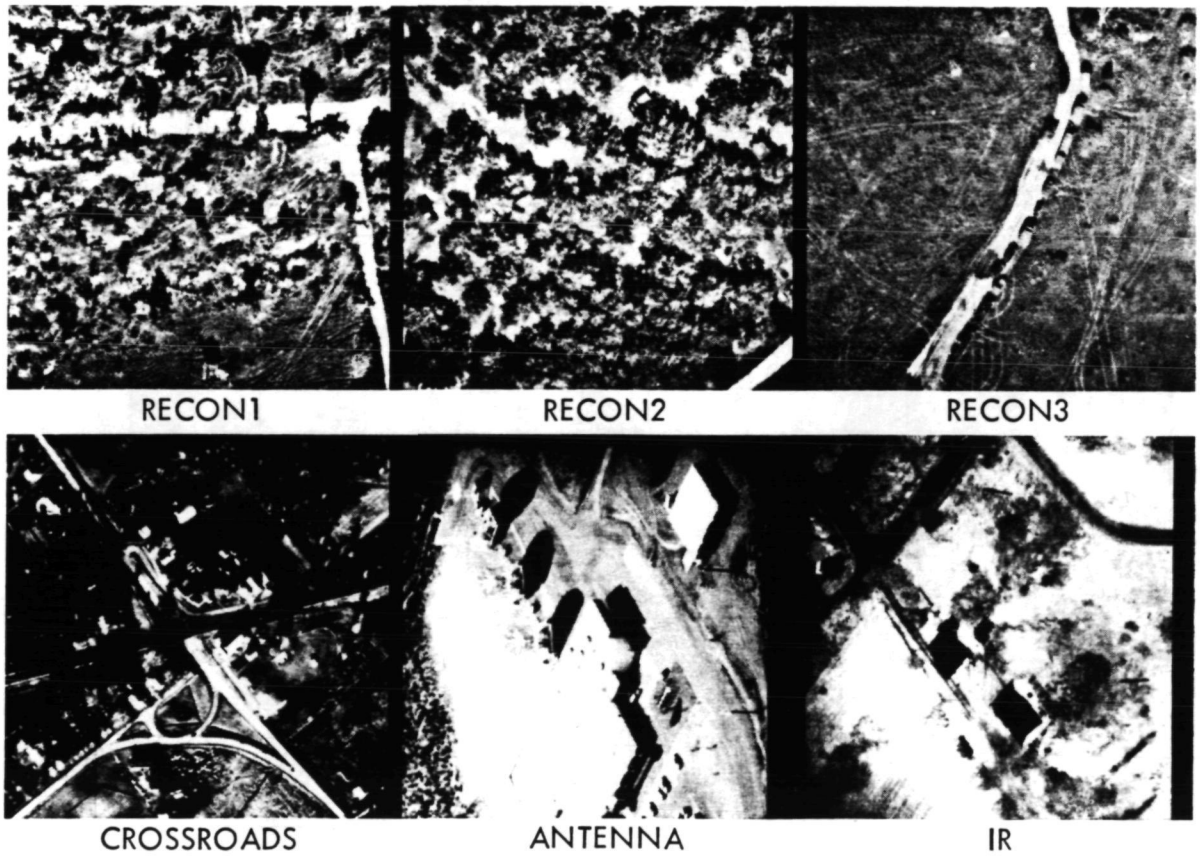

Fig. 16. Reconnaissance Images (512 x 512).

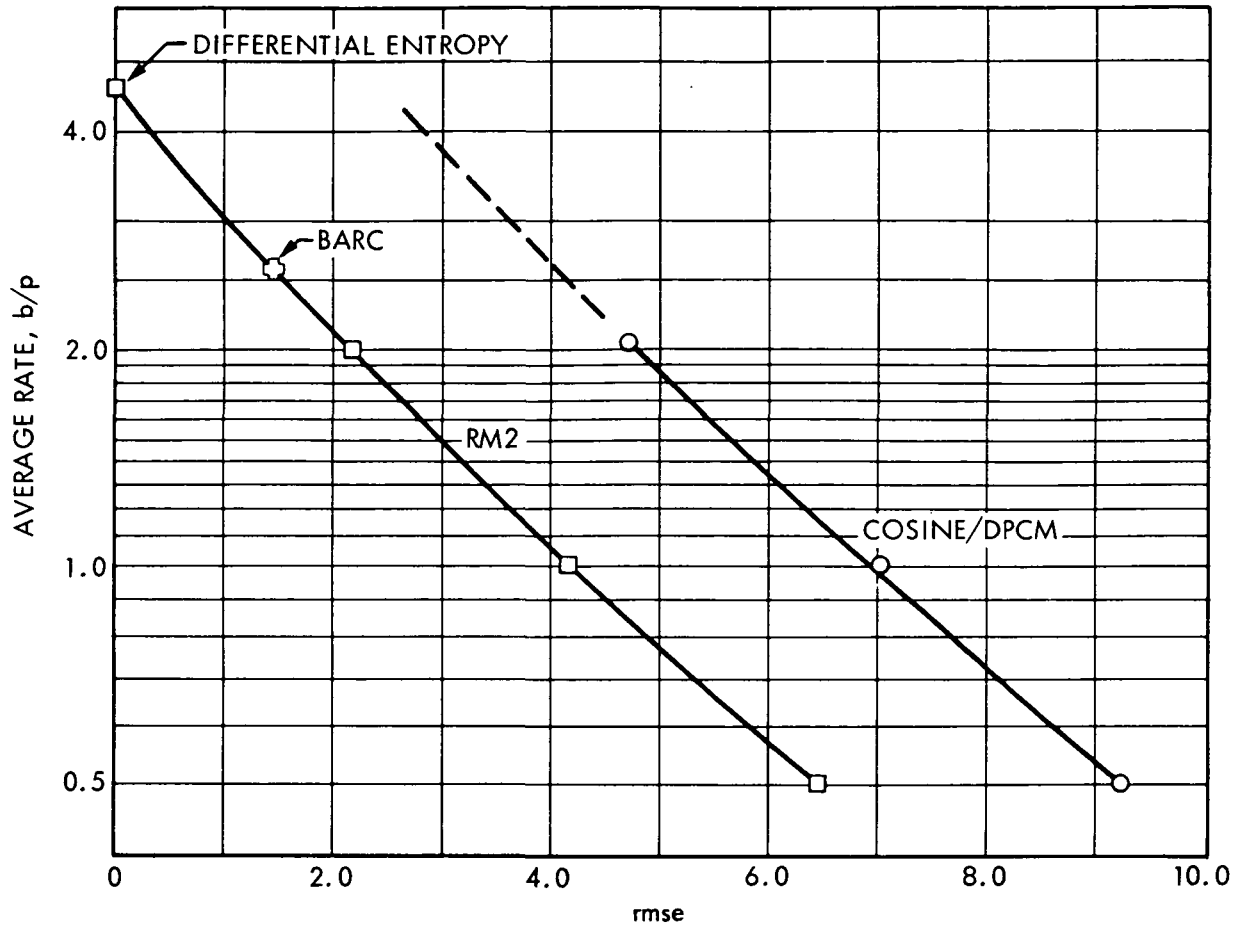

Fig. 17. RMSE Comparison: Crossroads Image.

Note that operation of the one-dimensional BARC algorithm[14] at 2.5 b/p lies on the RM2 performance curve for this image.† Further note that RM2 performance at higher-per-picture-element rates intersects at the image one-dimensional-differential entropy. This was true for all six reconnaissance images and is a natural consequence of the internal universal noiseless coding.[9]-[12]

The original crossroads image (512 x 512, 8 b/p) and an RM2 reproduction at 1 b/p is shown in Fig. 18. As a further example, Figure 19 visually illustrates RM2 performance on another reconnaissance image of Moffet Field, Ames Research Center (not in the test set of six). The 512 x 512, 8 b/p original is shown with RM2 reproductions at 1.6 b/p (5:1), 1.00 b/p (8:1) and 0.67 b/p (12:1). The differential entropy of this image is 4.5 b/p.

†BARC was noted earlier for its application to the Galileo Project.

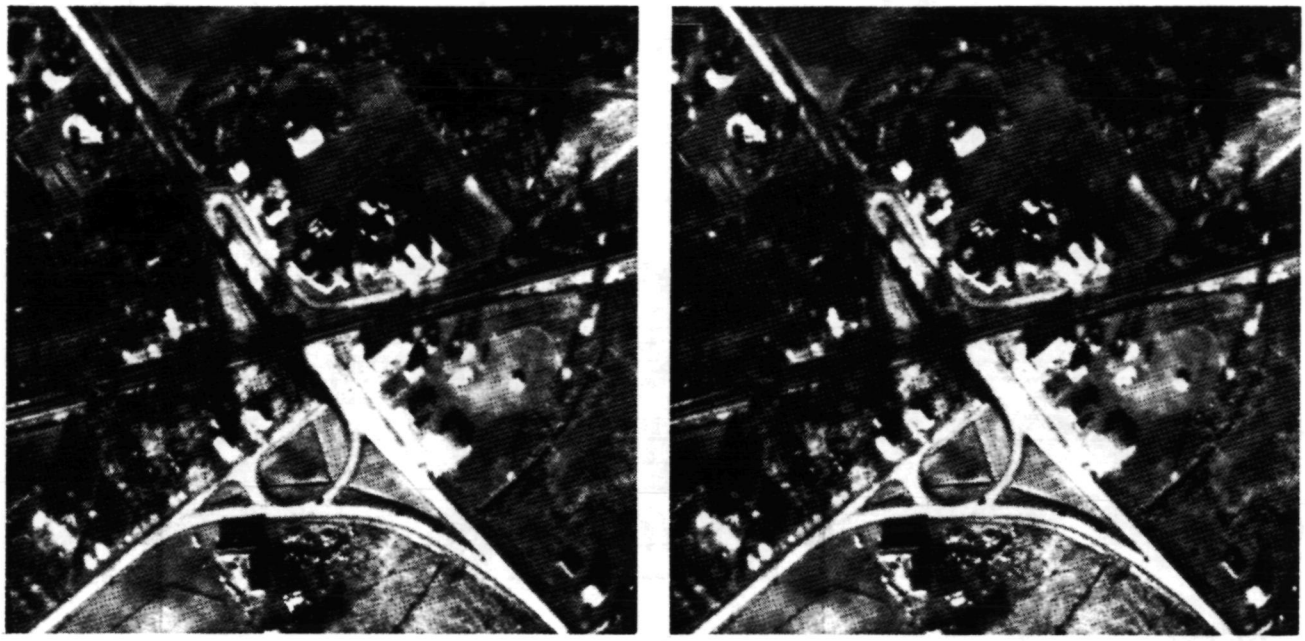

ORIGINAL 8 b/p RM2 1.0 b/p

Fig. 18. Crossroads Image.

Observe that all of the RM2 visual and rmse results noted in this section were run without any change in internal parameters other than selected rate.

RM2 Internal Structure

The preceding discussion principally focused on the system aspects and performance characteristics of RM2. It was noted that the end product of the global rate allocation structure was an allocation of bits to be used to represent individual subimages (e.g. 32 x 32 arrays). Any algorithm which can selectively and efficiently represent subimages with a broad range of rates (bits/subimage, b/p) could fit smoothly within this structure. The available per-sample rates need not be a continuous choice since any error in using a given number of bits can easily be reallocated to other subimages.[2] The Cox and Tescher's local rate control transform compression would certainly be a good high-performance option.[22] We will present the original RM2 local structure, illustrated in Fig. 20, which has provided some rather good results on a wide variety of data with what would appear to be considerably less computational complexity.

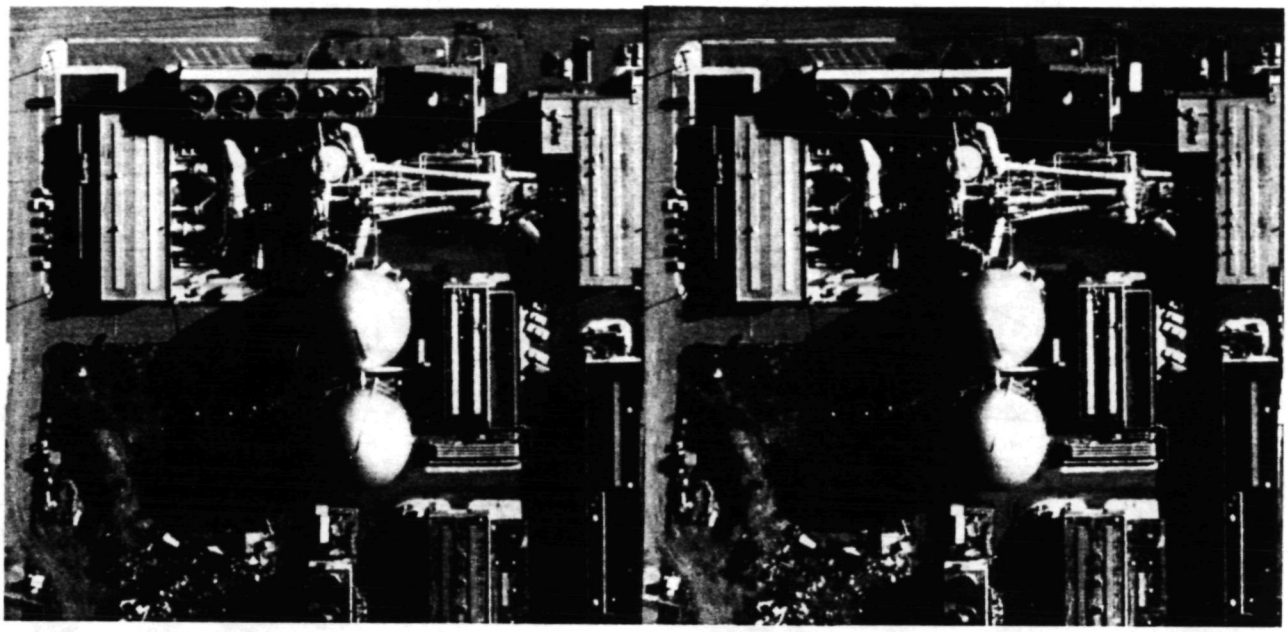

ORIGINAL 8 b/p

RM2 1.6 b/p

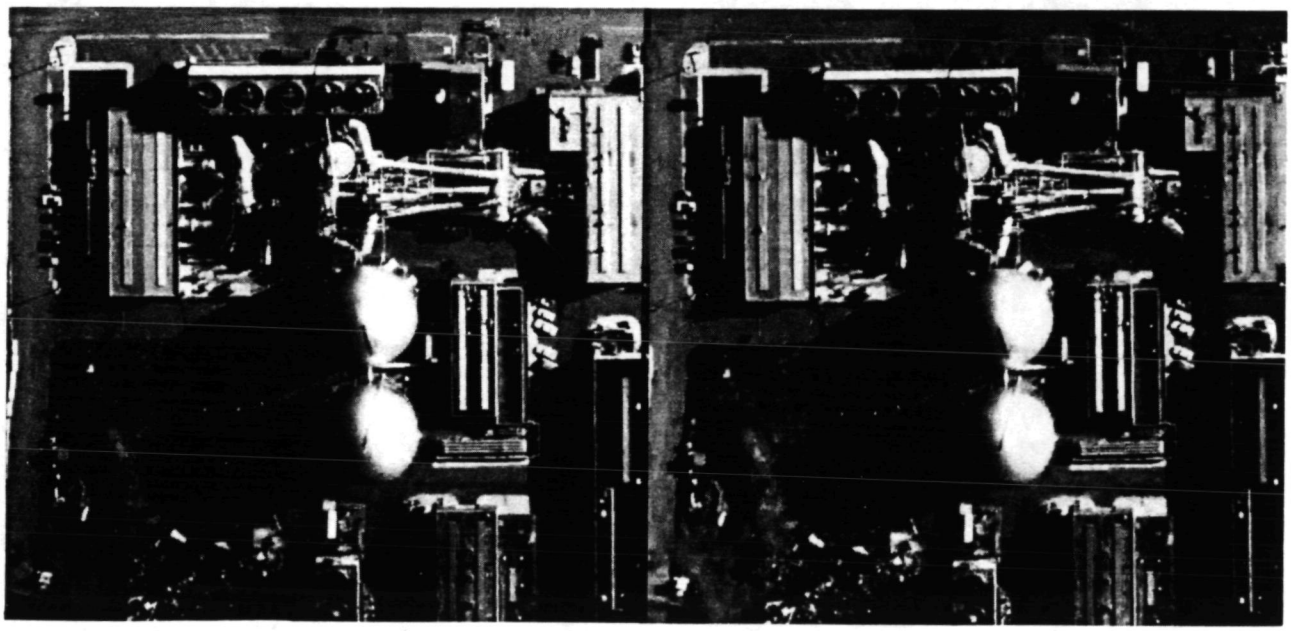

RM2 1.0 b/p

RM2 0.67 b/p

Fig. 19. Moffett Field Scene.

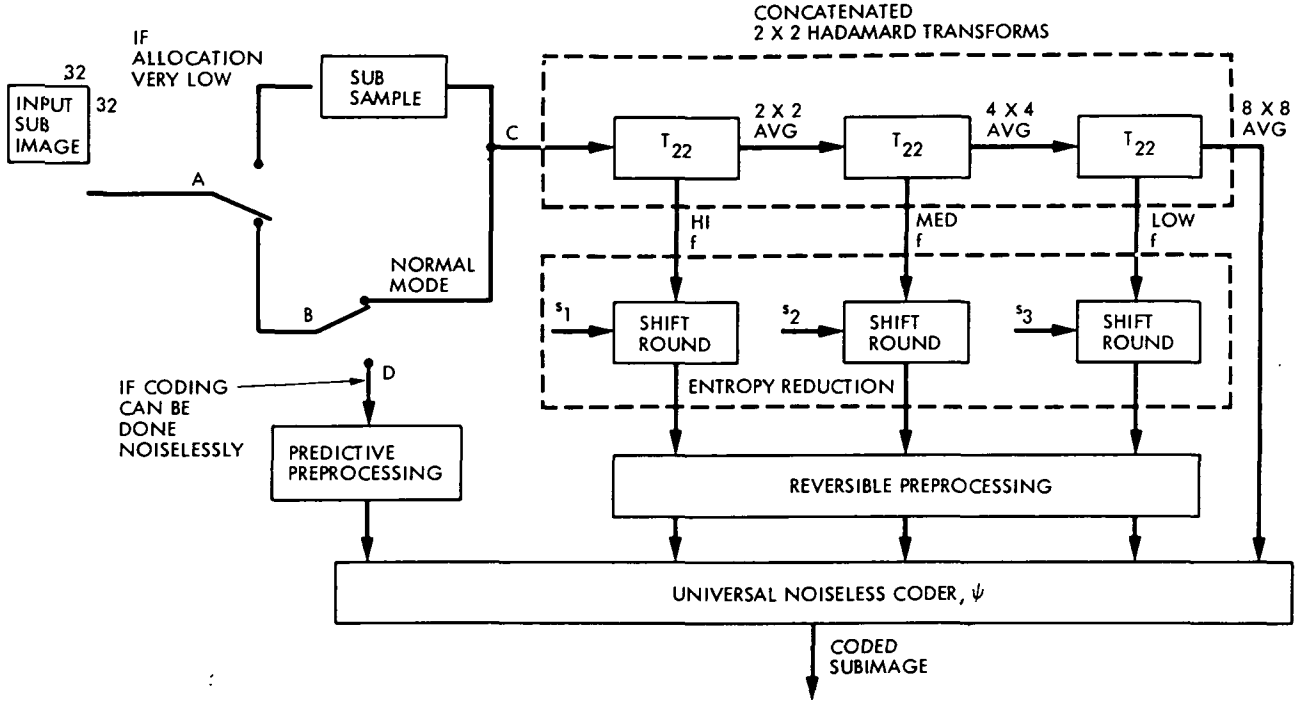

Fig. 20. RM2 Subimage Coding Structure.

Universal Noiseless Coder. As Fig. 20 shows, all data eventually pass through a box labeled ψ, called a universal noiseless coder, and are collectively the set of algorithms described in Refs. 10-12. Code operator ψ performs the function normally associated with Huffman coding[23] except that ψ is not dependent on a full knowledge of source statistics to be efficient. ψ provides efficient noiseless coding of memoryless sources for which only the probability ordering of input symbols is known, not their values. In this problem as in many other practical applications, this condition can be well approximated for real sources by preceding ψ with appropriate reversible preprocessing functions which serve to first remove correlation and second, to relabel symbols according to their likelihood of occurrence. ψ will then, without further knowledge, code at rates close to the average entropy for all entropies above zero.

High rate allocation. Returning now to Fig. 20, if the selected rate of a given subimage is sufficient to allow noiseless coding then that subimage will be efficiently coded at D by coupling one or two dimensional predictive preprocessing[13],[14] with the code operator ψ just noted. This same path also provides initial "data activity" estimates used in the rate allocation procedures noted earlier.

Transform mode. When the allocated bits for a subimage are not adequate to enable noiseless coding then that subimage undergoes simple entropy and dimensionality reducing transformations to enable coding at the desired rate. When allocated rates exceed roughly 0.75 b/p the input subimage is passed unchanged to point C whereas otherwise it is first subsampled to produce a slightly smaller two-dimensional array of picture elements at C (missing elements are later approximated by a decompressor using linear interpolation). In either case, the next step is the application of perhaps the (computationally) simplest transform used in practice.[2],[24] The overall transformation consists of a three-stage application of a two-by-two Hadamard transform T_{22}. In the first stage, T_{22} is applied to each two-by-two array making up the subimage of picture elements at C. The result for each application is a two-by-two average and three coefficients which contain the details on how the two-by-two differs from an all grey two-by-two. Only the averages are passed on to the next stage which must perform essentially the same function as the first, but on only one quarter the number of samples. The non-average T_{22} coefficients produced at the first stage are collectively denoted "high frequency" (HI f) coefficients in Fig. 20. The second stage generates an array of 4 x 4 averages (2 x 2 averages of 2 x 2 averages) and a collection of "medium frequency" coefficients (MED f). Again only the averages are passed on to yield an array of 8 x 8 averages and a collection of low frequency coefficients (LO f) at the third stage. This completes the transformation.

A floating point representation of the coefficients here would permit an error-free retrieval of the input data array at C by reversing the transform process. But exact reconstruction is unnecessary for transformed data since this function is

essentially provided by direct noiseless coding at D. The purpose of this mode of processing is specifically for situations when the bit allocation is insufficient to permit noiseless coding. For practical applications our simulations have shown that, for 8 b/p input data, very minor and acceptable degradation occurs if all transform levels are maintained at a linearly quantized 10-bit accuracy.

Efficient noiseless coding of transform coefficients at this full 10-bit precision can nevertheless be provided by again applying universal noiseless coder ψ. The required preprocessing can be accomplished by a simple relabeling for probability of occurrence since all coefficients are consistently characterized by unimodal distributions about zero.† A practical means of reducing the bits needed to code a subimage is obtained by selectively reducing the linear quantization at each transform level before applying noiseless coder ψ.

Successive reductions in linear quantization produce narrower transform distributions and hence lower entropies but do not alter the unimodal characteristics. Hence, the same reversible preprocessing (relabeling) needed for ψ applies to <u>all</u> transform levels and <u>any</u> reduction in linear quantization. A subimage can be coded closely to a prescribed number of bits by selecting the right combination of linear quantization reductions to gse. Since the relabeling and ψ coding are reversible operations, reconstructed quality will be as good as the chosen quantization options allow.‡ These operations are summarized in Fig. 20 where the function of quantization reduction is designated by the three boxes labeled shift/round. Here s_i, i = 1, 2, 3 denotes the selected reduction in linear quantization at transform level i.

†The numbers 0, 1, -1, 2, ... are mapped into the integers 0, 1, 2, 3, 4, ...

‡See Ref. 2 for slight improvements from an adaptive inverse using surrounding data.

IV. PERFORMANCE CURVES

The purpose of this section is to provide the coded (Gaussian) space channel performance curves used in the end-to-end system analysis of Section II. Additional notes and references to current implementation efforts are also provided.

Ideal Performance

Error probability versus signal-to-noise ratio curves for the selected channel coding configurations noted in Section II are shown in Fig. 21 where ideal receiver operating conditions are assumed.† Signal-to-noise ratio is plotted in dB as the received-energy-per-information-bit, E_b, per noise-spectral-density N_0.

Systems 1-4. Bit error probabilities, $\overline{P}_b$ are shown for the classic uncoded channel[25] (system 1 in Section II), a channel incorporating convolutional coding/Viterbi decoding (system 3) and a concatenated convolutional/Viterbi-Golay channel (gse portion of system 4).

The convolutional code assumed is a constraint length K = 7, rate $1/\nu = 1/2$ code and is the principal code used in today's deep space missions such as Voyager and Galileo. The graphs assume Viterbi decoding with 3 bits of receiver quantization, a capability currently available in the Deep Space Network (DSN) receiving stations ($\nu = 3$ is also available). Further details on the DSN capabilities can be found in Ref. 26. The characteristics of this code have been exhaustively treated in the literature for a broad range of applications. The graphs shown here correspond to various test results simulating DSN conditions[17],[27] and are little different than first reported by Heller and Jacobs.[5]

The interleaved Golay concatenation scheme which is much less well known is described in Ref. 3. For our purposes here it suffices to note that the modified Golay code itself is a 3 error-correcting binary block code with 12 bits of parity for each 12 information bits.

Assumptions of performance curve operating points leading to the Table 1 specification of rate advantages are, in most cases, noted in the figure. The critical $\{P_b, E_b/N_0\}$ points for the uncoded link are $\{10^{-3}, 6.8\text{ dB}\}$ and $\{10^{-5}, 9.7\text{ dB}\}$ (not shown). The two points assumed for the convolutional channel are $\{5 \times 10^{-3}, 2.3\text{ dB}\}$ and $\{10^{-5}, 4.8\text{ dB}\}$.

†Coherent demodulation of a square-wave subcarrier.

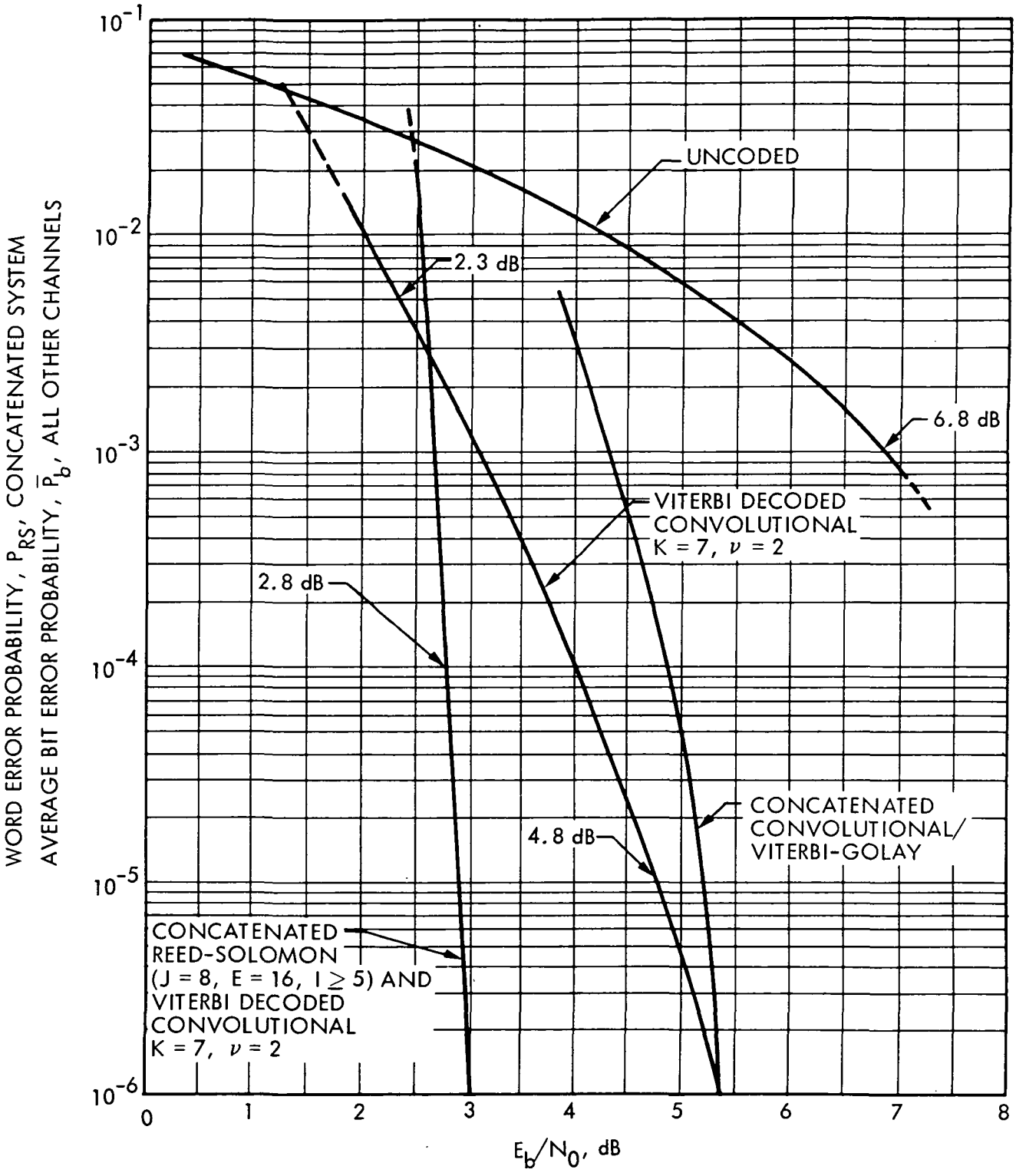

Fig. 21. Performance Curves.

Recall that the purpose of the concatenated convolutional/Viterbi-Golay channel was to enable system 4 in Fig. 5 to more efficiently satisfy the disparate error rate requirements of (uncompressed) imaging and a relatively error sensitive class of data called general science and engineering data (gse).

As a consequence of the 100 percent parity overhead the concatenated conv/Viterbi-Golay channel operates at an E_b/N_0 which is 3 dB above the operating point of the "inner" convolutional channel. Then from the performance curves of Fig. 21 we see that if the inner convolutional channel is operated at $\{5 \times 10^{-3}, 2.3 \text{ dB}\}$, thus meeting imaging requirements, the concatenated channel operates at $\{\leq 10^{-5}, 5.3 \text{ dB}\}$ thus meeting gse requirements.

In a similar argument, the Golay code in system 2 of Fig. 3 will meet the same gse requirements when the "inner" uncoded channel is operated at $\{10^{-3}, 6.8 \text{ dB}\}$. The corresponding performance curve is not shown in Fig. 21.

RS/Viterbi. The performance curve for an interleaved Reed-Solomon (RS) block code concatenated with the same $K = 7$, $\nu = 2$ convolutional/Viterbi channel as described for system 5 is shown in Fig. 21. The results are rather dramatic.

Based on Odenwalder's original studies in Refs. 27 and 28 the selection of practical code parameters is fairly obvious.[2] The chosen code is by the classic definition in Ref. 29 an $E = 16$ symbol error-correcting RS code with symbols defined over GF(256) (i.e., $J = 8$ bit symbols) and a code word length of 255 symbols (2040 bits). Because of the burstiness of Viterbi decoder error characteristics the RS code should be interleaved for best performance as was the Golay in system 4. Simulation studies by Odenwalder[30] and Liu[17] showed that performance equivalent to ideal (infinite) interleaving could be achieved with interleaving depths $I \geq 5$. The performance curves in Fig. 21 reflect the results of those studies. The relative merit of two forms of interleave architecture on compressed imagery is discussed in Ref. 2.

RS word error probability P_{RS} is shown in Fig. 21 rather than bit error probability since it better characterizes the effects of the concatenated channel. The channel is simply clean as long as an RS word contains no more than $E = 16$ symbol errors. When that happens seventeen or more scattered symbol errors will occur in the decoded output. Section II system considerations assumed an operating point of 2.8 dB and $P_{RS} = 10^{-4}$. At this operating point the channel is clean except for

an error event once every 2×10^7 bits or equivalently, once every sixteen Voyager images compressed 4 to 1. Note that 2.8 dB is only 0.5 dB above the operating point for uncompressed imaging on the convolutional channel, clearly a small price to derive the significant efficiencies of sophisticated data compression.

Our motivation for identifying the concatenated RS/Viterbi channel has, until now, been solely for its capability to provide significant net gains in information rate for deep space missions when coupled with data compression. However, it has long been noted that operation of the deep space network at maximum "tolerable" error rates incurs a difficult-to-quantify penalty in mission distribution and processing costs. Note that since the RS/Viterbi performance curve is so steep, an additional reduction in data rate by only 5 percent (0.2 dB E_b/N_0) would reduce error events in 4:1 compressed Voyager images to once every 1600 images, truly earning the label of "virtually error-free" communication.[2] By comparison, the convolutional channel alone would require an additional data rate reduction by a factor of 3 to achieve roughly equivalent performance. Thus combined with packet telemetry concepts[31] the RS/Viterbi channel in addition offers a practical vehicle for achieving reduced ground processing and distribution costs.

Non-Ideal Operating Conditions

The effect of various non-ideal receiver operating conditions on the performance of the convolutional/Viterbi channels was first characterized by Heller and Jacobs.[5] These results were later extrapolated to the concatenated RS/Viterbi channels by Rice.[2] Odenwalder verified and extended the latter conclusions by simulation.[29] More complete and exhaustive simulation measurements were recently compiled by Liu[32]-[33] using test equipment which closely models DSN characteristics. The major conclusion from these investigations is that the advantages of the concatenated system over convolutional/Viterbi alone increase significantly under non-ideal conditions when error rates of less than 10^{-4} are desired.

Additional theoretical performance considerations of the concatenated channel using phased array antennas are also treated by Liu in Ref. 33.

Implementation

We have carefully avoided any detail on the precise algebraic definition of the Reed-Solomon codes of interest and will continue to do so. However, there are many subtle differences in code definition which leave channel performance unchanged from Fig. 21 but influence the corresponding encoder and decoder implementations. Such considerations remain as the primary issue of standardization efforts.

Encoders. Classically defined Reed-Solomon encoders meeting the severe mission requirements of Voyager and Galileo were implemented in 50 - 80 flight-qualified CMOS parts by Johnson.[34],[35] The Galileo version can operate at roughly 1 megabit/second.

More recently Berlekamp provided clever algebraic modifications which significantly reduced the required off-the-shelf parts count for future high data rate encoders.[36],[37] Carrying this goal one step further Liu has breadboarded a VLSI design which would reduce such an interleaved 1 megabit/sec encoder to 4 chips.[38]

Decoders. There has not been the same pressing need for decoder implementations (the necessity for a Voyager/Uranus decoder will occur almost a decade after the 1977 launch). However, both NASA and the European Space Agency (ESA) have recognized the power of the RS code treated here, with and without an inner convolutional channel. In particular, they and others have recognized potential applications involving data rates in excess of 100 megabits/second. As such the computational requirements of a decoder become the driving concern. ESA is currently recommending that the RS code be defined over GF(257) instead of GF(256), as we have thus far assumed, in order to capitalize on a potential computation advantage afforded by Fermat primes.[38],[39],[40] The arguments are presented by Best and Roefs in Ref. 41. In either case code performance is, for all practical purposes, identical.

REFERENCES

(1) R. F. Rice, "Channel coding and data compression system considerations for efficient communication of planetary imaging data," Chapter 4, Technical Memorandum 33-695. Jet Propulsion Laboratory, Pasadena, CA, June 15, 1974.

(2) R. F. Rice, "An advanced imaging communication system for planetary exploration," Vol. 66 SPIE Seminar Proceedings, Aug. 21-22, 1975, pp. 70-89.

(3) L. D. Baumert and R. J. McEliece, "A Golay-Viterbi concatenated coding scheme for MJS'77," JPL Technical Report 32-1526, Vol. XVIII, pp. 76-84, Dec. 1973.

(4) A. J. Viterbi, "Convolutional codes and their performance in communication systems," IEEE Trans. Commun. Technol., Vol. COM-19, part II, Oct. 1971, pp. 751-772.

(5) J. A. Heller and I. M. Jacobs, "Viterbi decoding for satellite and space communication," IEEE Trans. Commun. Technol., Vol. COM-19, part II, Oct. 1971, pp. 835-848.

(6) J. Cutts and L. Lebofsky, "Evaluation of the RM2 image data compression technique for outer planet missions with the Pioneer spacecraft," submitted to Jet Propulsion Laboratory by Planetary Science Institute, Pasadena, CA, Final. Rep., Contract 954152, Nov. 1975.

(7) R. Kraus, "Effects of data compression on cloud motion measurement in planetary images," submitted to Jet Propulsion Laboratory by the Univ. of Wisconsin, Final Report, Contract 955856, June 1981.

(8) J. Cutts, K. Blasius, B. Lewis, J. Helu', "Modular data transport system data compression evaluation," submitted to the Jet Propulsion Laboratory by the Planetary Science Institute, Pasadena, CA, Final Report, Contract IC708842, June 1980.

(9) R. F. Rice, J. R. Plaunt, "Adaptive variable length coding for efficient compression of spacecraft television data," IEEE Trans. Commun. Technol., Vol. COM-19, Part I, Dec. 1971, pp. 889-897.

(10) R. F. Rice, "Some practical universal noiseless coding techniques," JPL Publication 79-22. Jet Propulsion Laboratory, Pasadena, CA, March 15, 1979.

(11) R. F. Rice, "Practical universal noiseless coding," SPIE Symposium Proceedings, Vol. 207, San Diego, CA, August 1979.

(12) R. F. Rice, A. Schlutsmeyer, "Software for universal noiseless coding," Proceedings of the 1981 International Conference on Communications, Denver, Colorado, June 1981.

(13) R. F. Rice, A. P. Schlutsmeyer, "Data compression for NOAA weather satellite systems," Vol. 249, Proceedings, 1980 SPIE Symposium, San Diego, CA, July 1980.

(14) R. F. Rice et al, "Block adaptive rate controlled image data compression," Proceedings of 1979 National Telecommunications Conference, Washington, D.C., Nov. 1979.

(15) R. F. Rice, "Potential end-to-end imaging information rate advantages of various alternative communication systems," JPL Publication 78-52. Jet Propulsion Laboratory, Pasadena, CA, June 15, 1978.

(16) R. F. Rice, "Comparative information rate advantages of alternative deep space communication systems," Proceedings of the International Conf. on the Performance of Data Communication Systems and Their Applications, Paris, France, Sept. 1981.

(17) K. Y. Liu, J. J. Lee, "An experimental study of the concatenated Reed-Solomon/Viterbi channel coding system performance and its impact on space communications," JPL Publication 81-58. Jet Propulsion Laboratory, Pasadena, CA, June 15, 1981.

(18) R. F. Rice, "A concept for dynamic control of RPV information system parameters," Proceedings of the 1978 Military Electronics Exposition, Anaheim, CA, Nov. 1978.

(19) R. F. Rice, "RM2: rms error comparisons," Technical Memorandum 33-804. Jet Propulsion Laboratory, Pasadena, CA, Sept. 15, 1976.

(20) C. Wu, R. F. Rice, V. C. Tyree, "RHD image compressor," NASA Tech. Brief NPO14041, Oct. 1976.

(21) P. Whiteman et al, "Hardware systems design of an airborne video bandwidth compressor for the RPV," Proceedings of the 1981 SPIE Symposium, Vol. 301, San Diego, CA, Aug. 27-28, 1981.

(22) R. V. Cox and A. G. Tescher, "Channel rate equalization techniques for adaptive transform coders," SPIE Seminar Proceedings, Vol. 87, Aug. 1976, pp. 239-246.

(23) D. A. Huffman, "A method for the construction of minimum-redundance codes," Proceedings of the IRE, Sept. 1952, pp. 1098-1101.

(24) R. F. Rice, "RM2: transform operations," Technical Memorandum 33-680. Jet Propulsion Laboratory, Pasadena, CA, March 1, 1974.

(25) J. M. Wozencraft and I. M. Jacobs, Principles of Communication Engineering, New York: Wiley, 1965.

(26) "Deep space network/flight project interface design handbook," JPL Document 810-5, Rev. D. Jet Propulsion Laboratory, Pasadena, CA, (JPL Internal Document), Sept. 15, 1980.

(27) J. P. Odenwalder, "Optimum decoding of convolutional codes," PhD dissertation, Syst. Sci., Dept., Univ. of California, Los Angeles, 1970.

(28) J. P. Odenwalder et al, "Hybrid coding systems study," submitted to NASA Ames Res. Ctr. by Linkabit Corp., San Diego, CA, Final Report., Contract NAS2-6722, September 1971.

(29) R. G. Gallager, Information Theory and Reliable Communication, New York: Wiley, 1968.

(30) J. P. Odenwalder, "Concatenated Reed-Solomon/Viterbi channel coding for advanced planetary missions: analysis, simulations and tests," submitted to the Jet Propulsion Laboratory by Linkabit Corp., San Diego, CA, Final Report, Contract 953866, December 1, 1974.

(31) A. Hooke, "User-oriented end-to-end transport protocols for the real-time distribution of telemetry data from NASA spacecraft," Proceedings of the SPIE Spring Symposium, April 1979.

(32) K. Y. Liu and L. T. Woo, "The effects of tracking phase error on the performance of the concatenated Reed-Solomon Viterbi channel coding system," Proceedings of the 1980 National Telecommunications Conference, Houston, Texas, November 30, 1980.

(33) K. Y. Liu, "The effects of receiver tracking phase error on the performance of the concatenated Reed-Solomon/Viterbi channel coding system," JPL Publication 81-62. Jet Propulsion Laboratory, Pasadena, CA., Sept. 1, 1981.

(34) D. Johnson, "Voyager flight data system," JPL Report MIS77-4-2006. Jet Propulsion Laboratory, Pasadena, CA, (JPL Internal Document), March 1978.

(35) D. Johnson, "Galileo solid state imaging subsystem," JPL Report GLL 4-2036. Jet Propulsion Laboratory, Pasadena, CA, (JPL Internal Document), Sept. 18, 1979.

(36) E. Berlekamp, "Technical proposal for a low-power Reed-Solomon encoder/interleaver using about 30 cmos IC's," submitted to the Jet Propulsion Laboratory by Cyclotomics, Inc., RFP No. BP-6-9007.

(37) M. Perlman, J. Lee, "Reed-Solomon encoders – conventional versus Berlekamp's architecture," JPL Publication 82-71 (to be published). Jet Propulsion Laboratory, Pasadena, CA.

(38) K. Y. Liu, "Architecture for VLSI design of Reed-Solomon encoders, JPL Publication 81-87. Jet Propulsion Laboratory, Pasadena, CA., Sept. 1981.

(39) K. Y. Liu, I. S. Reed, T. K. Truong, "High radix transforms for Reed-Solomon codes over Fermat primes," IEEE Trans. on Inform. Theory, Vol. IT-23, No. 6, Nov., 1977.

(40) I. S. Reed et al, "Fast transforms for decoding Reed-Solomon codes," IEEE Proceedings, Vol. 128, part F, No. 1, Feb. 1981.

(41) M. R. Best, H. H. A. Roefs, "Technical assistance telemetry channel coding investigation," Technical Report TR 81044'L. National Aerospace Laboratory NLR, Amsterdam, The Netherlands, April 15, 1981.

NASA–JPL–Coml., L.A., Calif.